



Article

Synthesis and Catalytic Activity in the Hydrogenation Reaction of Palladium-Doped Metal-Organic Frameworks Based on Oxo-Centered Zirconium Complexes

Rose K. Baimuratova ¹, Anastasia V. Andreeva ^{1,2}, Igor E. Uflyand ^{3,*}, Gennadii V. Shilov ¹, Farida U. Bukharbayeva ⁴, Alima K. Zharmagambetova ⁴ and Gulzhian I. Dzhardimalieva ^{1,5}

¹ Federal Research Center of Problems of Chemical Physics and Medicinal Chemistry of the Russian Academy of Sciences, Chernogolovka, 142432 Moscow, Russia

² Faculty of Fundamental Physical and Chemical Engineering, Lomonosov Moscow State University, GSP-1, 1 Leninskiye Gory, 119991 Moscow, Russia

³ Department of Chemistry, Southern Federal University, 344090 Rostov-on-Don, Russia

⁴ Laboratory of Organic Catalysis, D.V. Sokolskiy Institute of Fuel, Catalysis, and Electrochemistry, Kunaev Str. 142, Almaty 050010, Kazakhstan

⁵ Moscow Aviation Institute, National Research University, 125993 Moscow, Russia

* Correspondence: ieufllyand@sfedu.ru; Tel.: +7-928-111-2880



Citation: Baimuratova, R.K.; Andreeva, A.V.; Uflyand, I.E.; Shilov, G.V.; Bukharbayeva, F.U.; Zharmagambetova, A.K.; Dzhardimalieva, G.I. Synthesis and Catalytic Activity in the Hydrogenation Reaction of Palladium-Doped Metal-Organic Frameworks Based on Oxo-Centered Zirconium Complexes. *J. Compos. Sci.* **2022**, *6*, 299. <https://doi.org/10.3390/jcs6100299>

Academic Editor: Konda Gokuldoss Prashanth

Received: 2 September 2022

Accepted: 8 October 2022

Published: 9 October 2022

Publisher's Note: MDPI stays neutral with regard to jurisdictional claims in published maps and institutional affiliations.



Copyright: © 2022 by the authors. Licensee MDPI, Basel, Switzerland. This article is an open access article distributed under the terms and conditions of the Creative Commons Attribution (CC BY) license (<https://creativecommons.org/licenses/by/4.0/>).

Abstract: Metal-nanocluster-doped porous composite materials are attracting considerable research attention, due to their specific catalytic performance. Here we report a simple, cheap, and efficient strategy for the preparation of palladium hydrogenation catalysts based on metal-organic frameworks (MOFs). It has been shown that the synthesis of Pd/MOF results in the formation of palladium nanoparticles uniformly fixed on the surface. The composition and structure of the resulting composites were studied using elemental analysis, DSC, TGA, XRD, TEM, and IR spectroscopy. Pd nanoparticles with an average diameter of 8–12 nm were successfully confined in the UiO-type MOFs, and the obtained nanocomposites exhibited abundant porosity, high stability, and a large surface area. It has been shown that the resulting catalytic systems with high activity, selectivity, and stability reduce phenylacetylene and allyl alcohol to styrene and propanol, respectively, in liquid-phase hydrogenation reactions.

Keywords: metal-organic frameworks; composites; nanoparticles; heterogeneous catalysts; hydrogenation reactions

1. Introduction

Hydrogenation is a widely used reaction in oil refining and industrial organic synthesis; for example, about 75% of industrial hydrogenation processes are carried out in the presence of Pd/C catalysts [1]. The use of palladium on various carriers is preferable from the point of view of a significant decrease in the activation energy of H–H bond cleavage on the palladium surface and the mobility of chemisorbed hydrogen [2]. However, at low temperatures of the hydrogenation process, the catalyst is very sensitive to various impurities present, for example, in the feedstock for hydrogenation [3]. This problem of catalyst poisoning, the loss of catalytic activity and/or selectivity over time, is essential in the practice of industrial catalytic processes and is enormously time-consuming and costly because of catalyst replacement and process shutdown [4]. Therefore, it is important to create hydrogenation catalysts with high activity, selectivity, and stability.

Such catalytic systems can be obtained by using supports of a completely new type in the field of chemistry and materials science: metal-organic frameworks (MOFs) [5,6]. The possibility of careful selection of the nature of the structure-forming element: the type of metal and its chelate environment, the organic bridging linker, its size and functionality, is an undoubted advantage of MOF in comparison with other types of porous materials,

since it allows the design of a nanoreactor space, the walls of which can be equipped with functional groups of various chemical natures in an optimal way for the selective transformation [7–11]. The most studied catalytic transformations involving MOFs are ligand, linker, and metal ion exchange reactions, substitution reactions, the functionalization of the organic ligand by postsynthetic methods, and the catalytic transformation of guest molecules [12–14]. The MOF-based catalyst systems demonstrated to date can be roughly divided into three types: (1) catalysts with catalytic domains on inorganic sites of MOFs, (2) catalysts whose catalyst sites are immobilized on organic linkers, and (3) catalysts whose catalytic sites are encapsulated in pores. Undoubtedly, MOF, as a new type of highly ordered porous material with a variable size, shape, and microenvironment of pores, is also a promising platform for creating heterogeneous catalysts by encapsulating noble metal nanoparticles (NPs) into pores, which would limit the migration and aggregation of metal clusters.

At present, the use of noble metal NPs introduced into the matrix of MOFs has been demonstrated for CO oxidation [15], the water-mediated Suzuki-Miyaura reaction [16], the Ullmann reaction [17], hydrogenation and isomerization of olefins [18], chemoselective reduction of the C=C bond in various α,β -unsaturated carbonyl compounds [19–21], hydrogenation of phenylacetylene [22,23], methoxycarbonylation of iodobenzene [24], hydrogenation of nitrophenol to aminophenol [25], etc. Thus, we can conclude that the possibility of using MOFs in catalysis today knows no bounds, and impressive progress has already been made in using the porous system of MOFs as heterogeneous catalysts. At the same time, a number of scientific problems remain, the solutions to which will make it possible to use heterogeneous catalysts based on MOFs on an industrial scale: (1) the search for and creation of thermally and hydrolytically stable MOFs; (2) the development of efficient scalable activation methods (for many MOFs, a huge remaining trend is structure collapse upon removal of solvent molecules, counterions, or additional cocrystallizing organic molecules from the cavity); (3) the development of approaches that make it possible to control the morphology, topography, and dispersity of NPs formed on the MOF surface. In this regard, the previously developed method for the preparation of hybrid heterogeneous catalysts, which are polymer-doped metal NPs uniformly fixed on the surface of an inorganic support, turned out to be convenient [26,27]. In addition, a promising strategy in the literature is the creation of composite materials based on carbon nitride [28] or graphene oxide [29] to obtain materials with a synergistic effect of the matrix and palladium NPs.

Therefore, this work is aimed both at solving the problems associated with the creation of catalytic hydrogenation systems based on a new type of porous materials that can work effectively under mild conditions, studying the stability of the MOF support structure and the composition of active sites and developing convenient scalable methods for obtaining such highly porous materials, and at assessing the competitiveness of the obtained heterogeneous MOF-based catalysts with the most well-known industrial analogs (Pd/C). As a promising platform for the support of catalytically active Pd, a series of MOFs of the UiO type was chosen as one of the most chemically and thermally stable MOFs known to the literature [30–32]. For the synthesis of a series of isoreticular MOFs, a low-temperature rational synthesis concept was used, using presynthesized hexanuclear oxohydroxocarboxylate blocks of the $[\text{Zr}_6\text{O}_4(\text{OH})_4(\text{RCOO})_{12}]$ type. Depending on the synthetic conditions, these nodes may possess Brønsted and Lewis acidic sites, which have been shown to catalyze various reactions, including hydrolysis, dehydration, and esterification, among others [18].

2. Materials and Methods

2.1. Materials

Ethanol, isopropyl alcohol, cyclohexene, phenylacetylene, and allyl alcohol of REAKHIM grades were dried according to standard methods. The purity was confirmed by HPLC. $\text{PdCl}_2 \cdot 4\text{H}_2\text{O}$ (chemically pure), ZrCl_4 (chemically pure), organic acids 1,4-benzenedicarboxylic ($\text{C}_8\text{H}_6\text{O}_4$), 2-aminobenzene-1,4-dicarboxylic ($\text{C}_8\text{H}_6\text{O}_4\text{-NH}_2$) and 2,6-naphthalenedicarboxylic ($\text{C}_{12}\text{H}_8\text{O}_4$) acids were purchased from Sigma Aldrich and were used without further purification.

2.2. Characterization Techniques

The content of C, H, and N was determined on a VarioMicrocube elemental analyzer (Elementar GmbH, Germany). The specific surface area of the samples, the average radius, and the pore size distribution were determined by low-temperature nitrogen adsorption (at 77 K) on an AUTOSORB-1 sorption analyzer (Quantachrome, United States) using a static volumetric method. Curves of differential scanning calorimetry (DSC) and thermogravimetric analysis (TGA) were recorded, using a METTLER TOLEDO DSC822e differential scanning calorimeter (Mettler Toledo, Switzerland) and a TGA/SDTA851e METTLER TOLEDO thermogravimetric analyzer (Mettler Toledo, Switzerland). The samples were heated in a nitrogen atmosphere at a heating rate of 10 K min^{-1} in the temperature range of 25–600 °C. Identification of functional groups and additional information on the type of coordination was carried out on an ALPHA IR spectrometer (Bruker Optik GmbH, Germany) with a spectral resolution of 2 cm^{-1} for a wavenumber range of 4000–350 cm^{-1} . An X-ray diffraction analysis (XRD) of the samples was performed on an Aeris Benchtop powder diffractometer in the range of scattering angles from 5 to 90° (scanning step in 2θ is 0.02°, radiation is $\text{CuK}\alpha$, $\lambda = 1.5405 \text{ \AA}$). Transmission electron microscopy (TEM) was performed using a transmission electron microscope (Tecnai Osiris FEI, Hillsboro, OR, USA). The Digital Micrograph, JEMS, TIA, and Image Scope programs were used to process and analyze images obtained with an electron microscope.

2.3. Synthesis Techniques

2.3.1. Synthesis of MOF of the UiO Type

In a typical synthesis, the calculated amount of the organic ligand, namely 1,4-benzenedicarboxylic, naphthalenedicarboxylic and 2-amino terephthalic acid, was dissolved in an ethanol solution with the addition of the calculated amount of potassium hydroxide. Zirconium oxoacetate was prepared in a separate reaction vessel. To do this, concentrated acetic acid was added dropwise to an aqueous solution of zirconium chloride. The pH was adjusted to 1.5 with 1 M NaOH solution. Since there is only a relatively small pH window where the Zr acetate complex predominates as the hexanuclear secondary structural unit $[\text{Zr}_6\text{O}_4(\text{OH})_4(\text{CH}_3\text{COO})_{12}]$, the mixture was kept at 55 °C for 180 min with constant stirring until the color changed from light pink to light yellow. The organic ligand solution was added to the resulting solution by stirring. The resulting precipitate was isolated by centrifugation at 4500 rpm, washed several times with absolute ethanol, and dried in a vacuum (10^{-3} Torr, 80 °C, 10 h).

2.3.2. Synthesis of Pd Doped Heterogeneous Catalysts

The synthesis of a heterogeneous catalyst was carried out based on the content of Pd 0.5 wt.%/g of support. In a typical procedure, PdCl_2 (0.094 mol) and KCl (0.2068 mol) in the presence of PEG-1500 (0.1 mmol) were dissolved in 100 mL of absolute ethanol. After complete dissolution by stirring on a magnetic stirrer, the calculated amount of MOF was added, and the mixture was refluxed until a dark color, characteristic of palladium reduction, formed. The resulting precipitate was isolated by centrifugation at 4500 rpm, washed several times with ethanol, and dried in a vacuum. The water adsorbed in the MOF pores was replaced with absolute ethanol using a Soxhlet apparatus (16 h, 100 °C), and ethanol was then removed from the pores by vacuum activation (16 h, 150 °C).

2.4. Catalytic Tests

2.4.1. Hydrogenation of Cyclohexene

The hydrogenation reaction of cyclohexene was chosen as a model reaction for the rapid determination of the activity of catalysts. The experiments were carried out in a non-flowing glass gradient-free thermostatic reactor of “the duck” type, in isopropyl alcohol at a cyclohexene concentration of $7 \times 10^{-3} \text{ mol/L}$, a constant hydrogen atmospheric pressure (0.1 MPa), and a temperature of 40 °C, under conditions of intensive shaking of the reactor (180–240 swings per minute). The catalyst weights were $0.10 \pm 0.05 \text{ g}$. Hydrogen was

supplied to the reactor from a calibrated receiver with a water seal. To determine the natural pressure of the gas, the partial pressure of the water vapor was subtracted from the total atmospheric pressure, and the gas volume was then brought to normal conditions. Before the introduction of cyclohexene, the catalyst was subjected to 15 min of treatment with hydrogen directly in the reactor, by stirring. The reaction rate was calculated graphically from the slope of the initial portions of the hydrogen consumption kinetic curves. In parallel experiments, the discrepancy did not exceed 5%.

2.4.2. Hydrogenation of Phenylacetylene and Allyl Alcohol

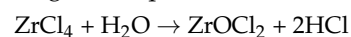
Hydrogenation was carried out in a non-flowing glass gradient-free thermostatic reactor of “the duck” type in ethanol (25 mL) at an atmospheric pressure of hydrogen and a temperature of 40 °C by intensive shaking of the reactor (600–700 swings per minute). The catalyst (0.05 g) was preliminarily treated with hydrogen directly in the reactor for 30 min with vigorous stirring, and then 0.25 mL of the substrate was introduced. The amount of substrate was taken, based on the absorption of 100 mL of hydrogen. The reaction rate was calculated from the change in hydrogen uptake per unit time. To assess the stability, hydrogenation was carried out cyclically, up to 5 times.

3. Results

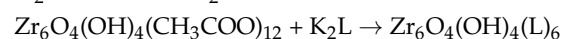
3.1. Synthesis of Pd-Doped Catalysts

The synthesis of target Pd-doped MOFs was carried out using exchange reactions of monotopic ligands in the in situ formed oxohydroxocarboxylate block of the $[\text{Zr}_6\text{O}_4(\text{OH})_4(\text{CH}_3\text{COO})_{12}]$ type for dicarboxylate (1,4-benzenedicarboxylic ($\text{C}_8\text{H}_6\text{O}_4$), 2-aminobenzene-1,4-dicarboxylic ($\text{C}_8\text{H}_6\text{O}_4\text{-NH}_2$) and 2,6-naphthalenedicarboxylic ($\text{C}_{12}\text{H}_8\text{O}_4$)) with the formation of the required structure. This process can be described by the system of the following reaction equations:

Stage 1. Preparation of hexanuclear zirconium acetate:



Stage 2. Reticulation of acetate residues into dicarboxylate ones:

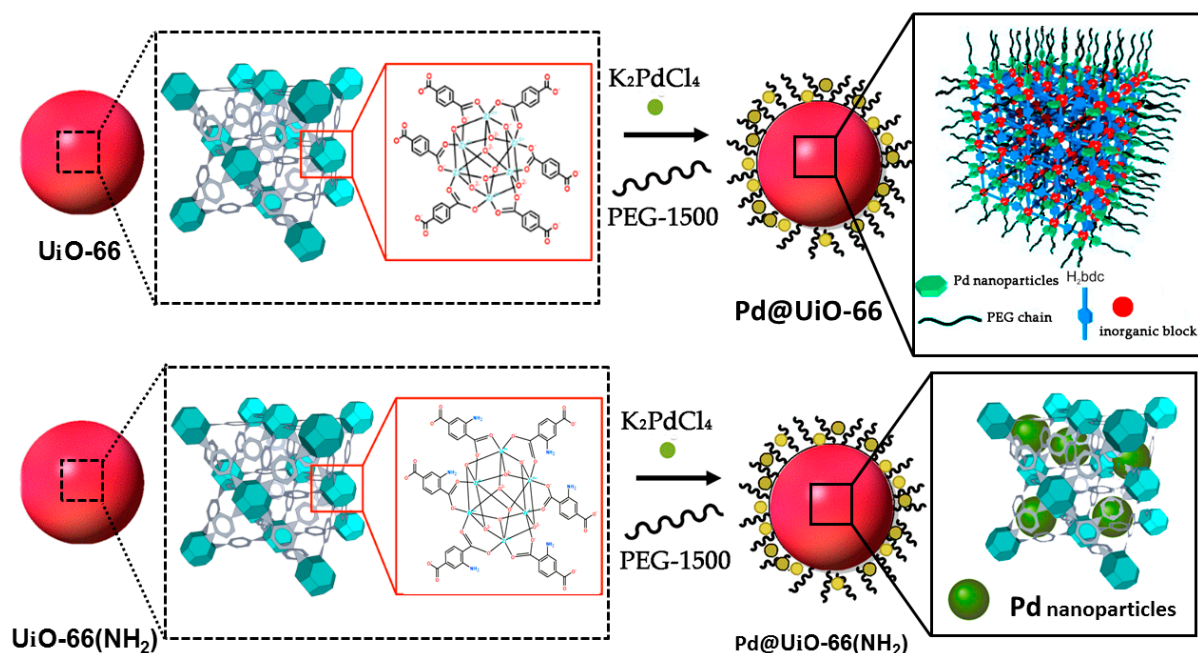


where H_2L is dicarboxylic acid.

Since there is only a relatively small pH window where the zirconium acetate complex predominates as a hexanuclear secondary structural unit [33], synthesis of the $\text{Zr}_6\text{O}_4(\text{OH})_4(\text{L})_6$ cluster was carried out at $\text{pH} = 1.5$.

Palladium was introduced into the MOF matrix by the chemical reduction of Pd(II) ions with PEG-1500. Polyethylene glycol in this case serves as both a reducing agent and a stabilizer for Pd(0) NPs, as shown by F.A. Harraz et al. [34]. Thus, the in situ formation of Pd(0) NPs can be schematically represented as follows (Scheme 1):

Based on the results of elemental analysis (Table 1), thermogravimetric analysis and DSC studies (Table 2, Figure 1), empirical formulas of the obtained MOFs are proposed.



Scheme 1. Schematic representation of the proposed strategy for obtaining catalysts based on UiO-66.

Table 1. Results of elemental analysis of the obtained MOFs based on zirconium oxoacetate.

Sample	Estimated Formula	Elemental Content [wt. %] (Found/Calc.)			
		C	H	N	Pd
1	Pd/Zr ₆ O ₄ (OH) ₄ (C ₈ H ₄ O ₄ -NH ₂) ₆ (H ₂ O) ₁₂	27.6/28.9	3.7/3.8	3.3/4.2	0.79
2	Pd/Zr ₆ O ₄ (OH) ₆ (C ₈ H ₄ O ₄) ₆ (H ₂ O) ₄	33.4/33.0	2.8/2.8	0/0	0.50
3	Pd/Zr ₆ O ₄ (OH) ₄ (C ₁₂ H ₆ O ₄) ₆ (H ₂ O) ₁₈	37.8/37.8	3.7/3.4	-	0.61

Table 2. Thermal properties of the prepared catalytic systems *.

Sample	T _{5%} [°C]	T _{10%} [°C]	T _{20%} [°C]	T _{30%} [°C]	T _{max} [°C]	Residual Weight at 600 °C [wt.%]
1	112	146	272	433	364	64.87
2	235	285	308	318	330	35.87
3	365	380	395	405	543	36.52

* T_{5%}, T_{10%}, T_{20%}, T_{30%}—temperatures of 5, 10, 20, and 30% weight loss, respectively; T_{max} temperature of the maximum decomposition rate according to the DTG curve.

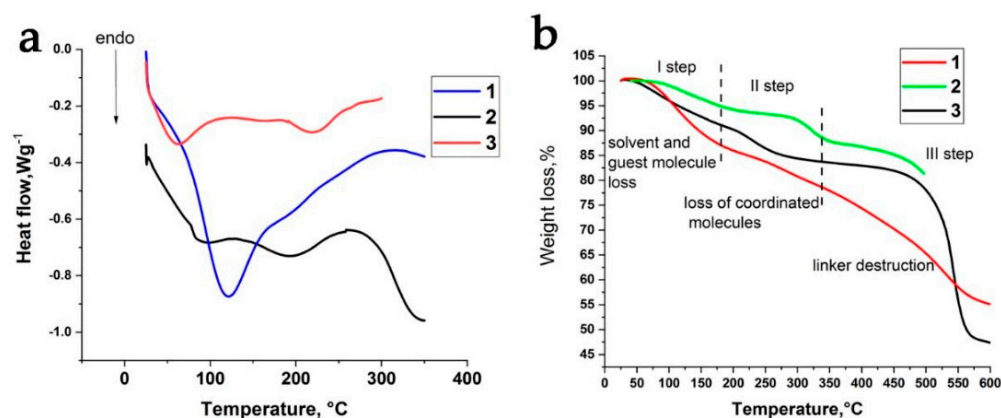


Figure 1. DSC (a) and TGA (b) curves for obtained samples: 1—Pd/Zr₆O₄(OH)₄(C₈H₄O₄-NH₂)₆(H₂O)₁₂; 2—Pd/Zr₆O₄(OH)₆(C₈H₄O₄)₆(H₂O)₄; 3—Pd/Zr₆O₄(OH)₄(C₁₂H₆O₄)₆(H₂O)₁₈.

According to the TGA curves, all obtained MOFs demonstrate three main stages of decomposition; the maximum decomposition rates for the second stage, according to the DTG curve, are observed above 300 °C, which indicates their high thermal stability. The first stage of the MOF decomposition, which proceeds up to 200 °C, is associated with the removal of physically adsorbed solvents. Such an elevated temperature indicates strong coordination interactions. The second stage of decomposition is accompanied by decarboxylation, according to the mass spectra of gaseous products (m/e 44 and m/e 28). The third stage of decomposition, which occurs above 380 °C, is accompanied by a deeper decomposition of the MOF framework with the formation of zirconium oxides.

In accordance with the IR spectroscopy data presented in Figure 2, MOFs have intense broad peaks in the region of 3600–3200 cm^{-1} , related to the stretching vibration of the -OH group. The stretching vibrations of the =C-H group appear in the region of 2950–2640 cm^{-1} . In the case of using amino terephthalic acid as an organic component, it was shown by IR spectroscopy that the band at 960–950 cm^{-1} indicates the formation of an amino complex with Pd by the polymer. Symmetrical stretching vibrations of the carbonyl group C=O in the MOF structure appear in the region of 1620–1550 cm^{-1} , asymmetric—at 1474–1415 cm^{-1} ($\Delta\nu_{\text{as}}(\text{COO})-\nu_{\text{s}}(\text{COO}) = 140\text{--}150 \text{ cm}^{-1}$). The decrease in the difference between the asymmetric and symmetric vibrations of the carboxyl group can be explained by the fact that the carboxylate ion coordinates with the metal in the bridging mode. The bands of C-N stretching vibrations inherent in aromatic amines appear at 1250 cm^{-1} , and upon the formation of a complex of palladium with an amino group, they shift to the region of 960–950 cm^{-1} . The peak at 768 cm^{-1} corresponds to the bending vibration =C-H in substituted benzene derivatives, and the peaks at 507–480 cm^{-1} correspond to vibrations of the Zr-O bond.

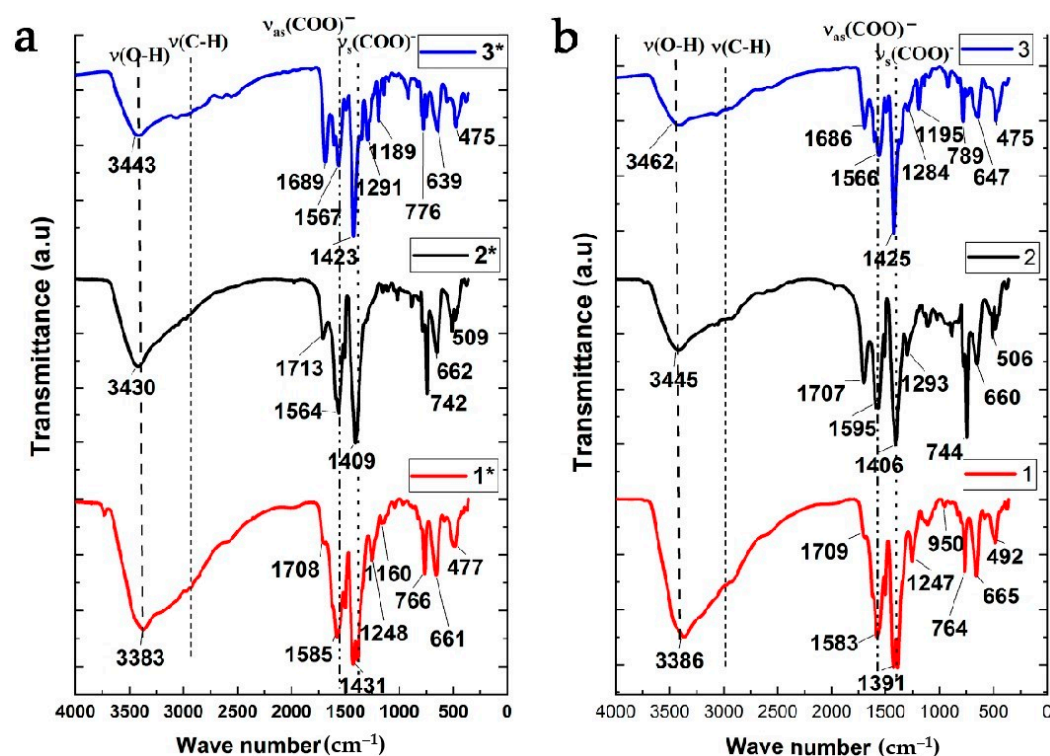


Figure 2. IR spectra of the resulting MOFs before (a) and after (b) inclusion of Pd NPs: 1—Pd/Zr₆O₄(OH)₄(C₈H₄O₄-NH₂)₆(H₂O)₁₂; 2—Pd/Zr₆O₄(OH)₆(C₈H₄O₄)₆(H₂O)₄; 3—Pd/Zr₆O₄(OH)₄(C₁₂H₆O₄)₆(H₂O)₁₈; 1*—Zr₆O₄(OH)₄(C₈H₄O₄-NH₂)₆(H₂O)₁₂; 2*—Zr₆O₄(OH)₆(C₈H₄O₄)₆(H₂O)₄; 3*—Zr₆O₄(OH)₄(C₁₂H₆O₄)₆(H₂O)₁₈.

Table 3 and Figure 3 show the results of low-temperature nitrogen adsorption of the samples. It can be seen that the obtained MOFs have segments of the S-shaped adsorption

isotherm, indicating the occurrence of polymolecular adsorption in mesoporous systems. Interestingly, the introduction of amino groups into the organic linker reduces the pore volume. The observed hysteresis loops are found in materials with slit-shaped pores.

Table 3. Specific surface area, pore volume and average pore size of the obtained catalysts.

Sample	S_{BET} [m ² /g]	V_p [cm ³ /g]	Average Pore Diameter [nm]	t Method		
				V_{micro} [cm ³ /g]	S_{micro} [m ² /g]	S_{external} [m ² /g]
1	558.9	0.47	5.68	0.11	257.0	302.0
2	359.6	0.86	3.78	0.014	39.1	320.5
3	400.0	0.65	4.73	0.025	64.8	335.1

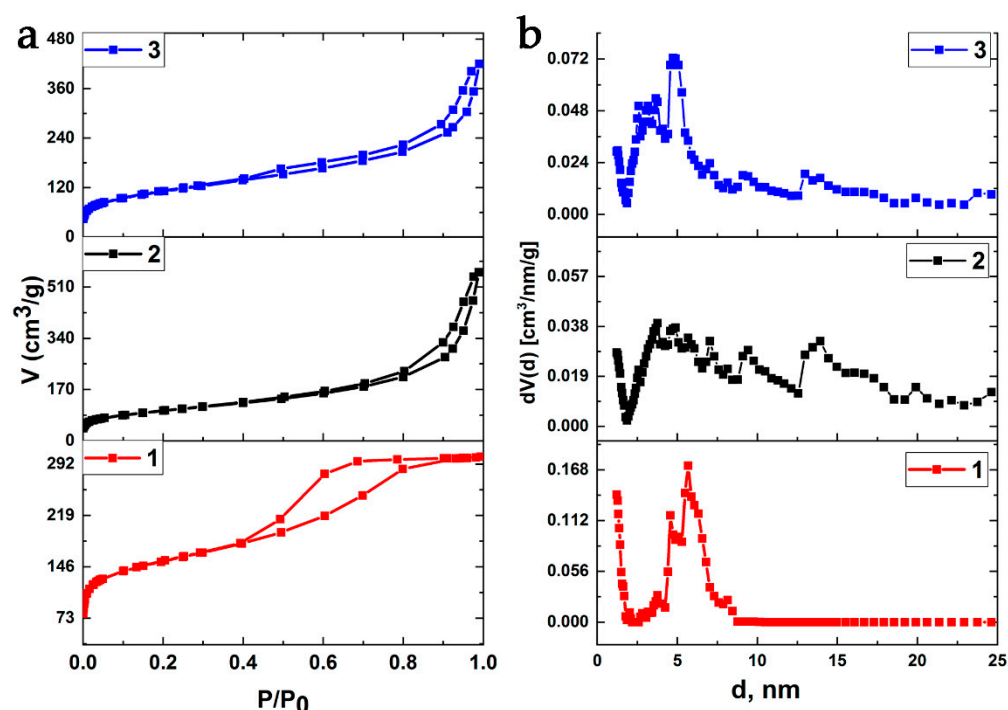


Figure 3. Nitrogen adsorption-desorption isotherms (a) and differential pore radius distribution calculated by DFT method (b) for activated samples: 1—Pd/Zr₆O₄(OH)₄(C₈H₄O₄-NH₂)₆(H₂O)₁₂; 2—Pd/Zr₆O₄(OH)₆(C₈H₄O₄)₆(H₂O)₄; 3—Pd/Zr₆O₄(OH)₄(C₁₂H₆O₄)₆(H₂O)₁₈.

The observed XRD patterns of the obtained MOF powders are shown in Figure 4. As can be seen from the presented XRD patterns, the narrow diffraction maxima indicate a predominantly crystalline phase state of the obtained MOFs, and the introduction of Pd NPs does not affect the XRD curve profile and the thermal stability of the carrier matrix. The Bragg reflection centered around 7° corresponds to the (111) reflection plane of the triclinic grating type [35]. Peaks at 16.37, 24.23, 21.77° for Zr₆O₄(OH)₆(C₈H₄O₄)₆(H₂O)₄ correspond to unreacted 2,6-naphthalenedicarboxylic acid ligand (CCDC 1422388). This may be due to the entrapment of ligand molecules in the MOF pores, and therefore it is difficult to purify, which also occurs for terephthalic acid [36].

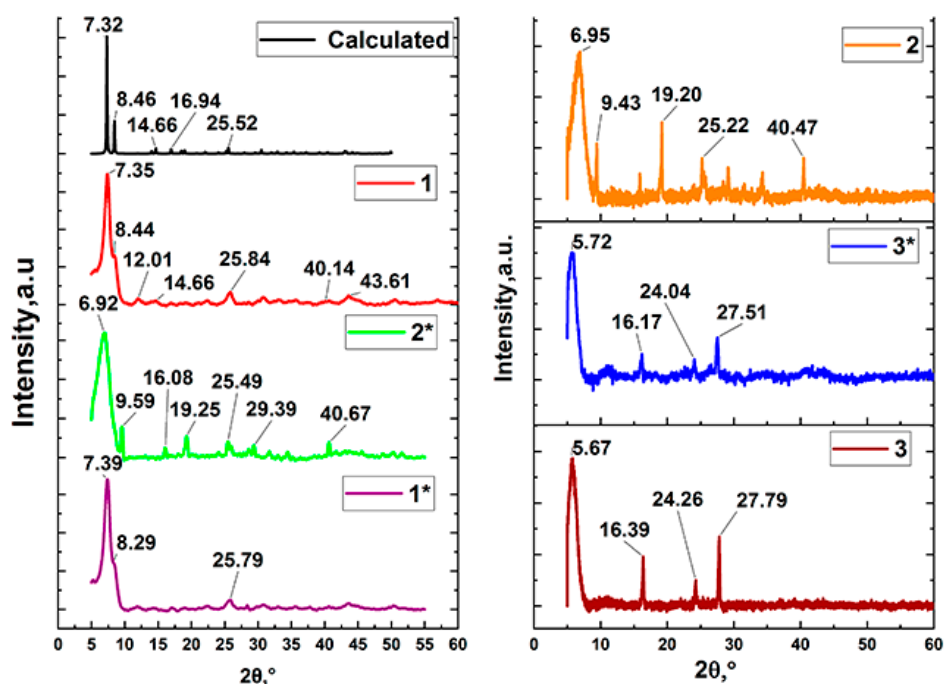


Figure 4. XRD patterns of the obtained MOFs before and after deposition of Pd NPs compared to calculated: 1—Pd/Zr₆O₄(OH)₄(C₈H₄O₄-NH₂)₆(H₂O)₁₂; 2—Pd/Zr₆O₄(OH)₆(C₈H₄O₄)₆(H₂O)₄; 3—Pd/Zr₆O₄(OH)₄(C₁₂H₆O₄)₆(H₂O)₁₈; 1*—Zr₆O₄(OH)₄(C₈H₄O₄-NH₂)₆(H₂O)₁₂; 2*—Zr₆O₄(OH)₆(C₈H₄O₄)₆(H₂O)₄; 3*—Zr₆O₄(OH)₄(C₁₂H₆O₄)₆(H₂O)₁₈.

The microstructure of the Pd/Zr₆O₄(OH)₄(C₈H₄O₄-NH₂)₆(H₂O)₁₂ and Pd/Zr₆O₄(OH)₆(C₈H₄O₄)₆(H₂O)₄ catalysts under study was studied by TEM. For these types of catalytic systems, due to the good catalytic activity, it was interesting to see the distribution of components relative to each other; for this, surface areas were mapped for the presence of Pd, C, Zr elements, using TEM. The results of the studies are shown in Figure 5. It can be seen that catalytically active Pd NPs are located on the surface of the Pd/Zr₆O₄(OH)₄(C₈H₄O₄-NH₂)₆(H₂O)₁₂ catalyst, mainly in the MOF pores only; it would seem that this is due precisely to the formation of an amino complex with Pd at the amino group of the organic linker, which was previously confirmed by IR spectroscopy. Subsequent reduction using a strong reducing agent such as sodium borohydride led to the construction of a nanoreactor space, the walls of which are equipped with a functional amino group and NPs of the catalytically active Pd, which in turn can be useful for the selective hydrogenation transformations. NPs of the catalytically active Pd are uniformly distributed over the surface of the Pd/Zr₆O₄(OH)₆(C₈H₄O₄)₆(H₂O)₄ catalyst, have a spherical shape, and dimensions of 8–12 nm. In the case of Pd/Zr₆O₄(OH)₄(C₈H₄O₄-NH₂)₆(H₂O)₁₂, the particle sizes range from 2 to 10 nm.

Comparison of micrographs of the TEM images of the surface of the catalysts shows that the surface morphology of the Pd/Zr₆O₄(OH)₆(C₈H₄O₄)₆(H₂O)₄ catalyst has a looser structure. In the intervals between blocks of aggregates, one can see systems of pore channels (Figure 6).

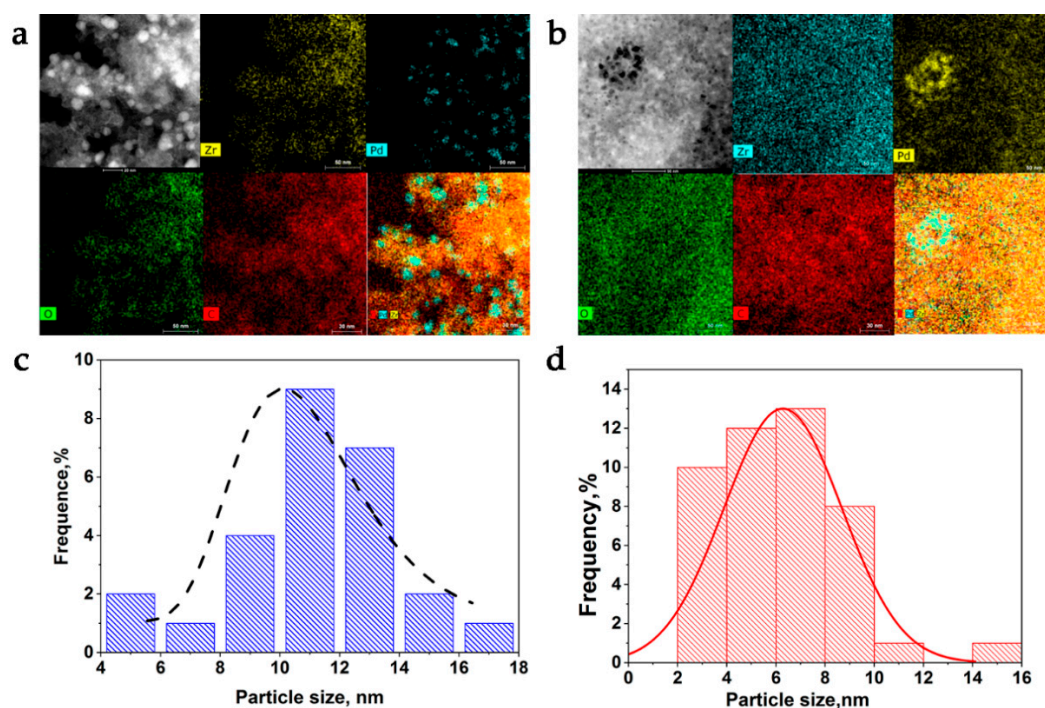


Figure 5. Catalyst surface mapping by elements (O, C, Zr and Pd) (a,b) and Pd NP size distribution histograms obtained from TEM images (c,d): (a,c)— $\text{Pd/Zr}_6\text{O}_4(\text{OH})_6(\text{C}_8\text{H}_4\text{O}_4)_6(\text{H}_2\text{O})_4$; (b,d)— $\text{Pd/Zr}_6\text{O}_4(\text{OH})_4(\text{C}_8\text{H}_4\text{O}_4\text{-NH}_2)_6(\text{H}_2\text{O})_{12}$.

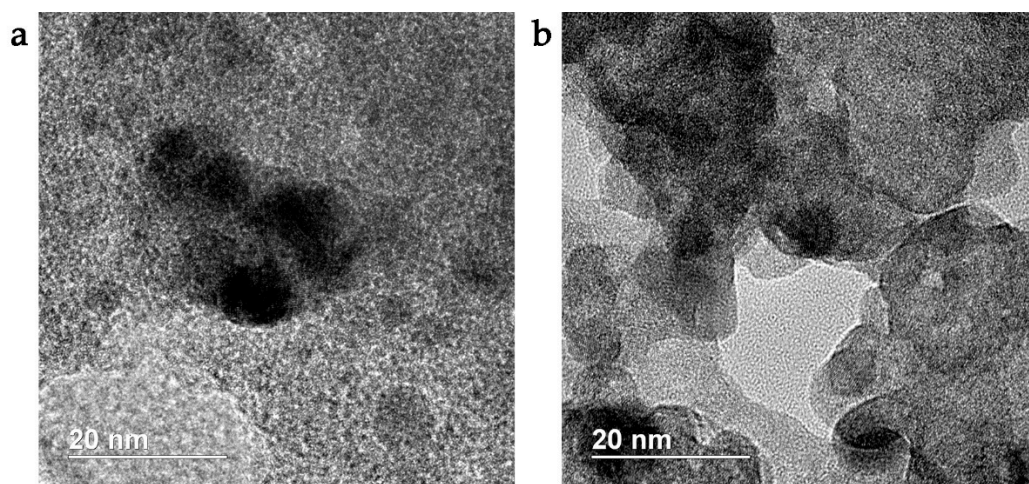


Figure 6. TEM images of the surface of catalysts: (a)— $\text{Pd/Zr}_6\text{O}_4(\text{OH})_4(\text{C}_8\text{H}_4\text{O}_4\text{-NH}_2)_6(\text{H}_2\text{O})_{12}$ and (b)— $\text{Pd/Zr}_6\text{O}_4(\text{OH})_6(\text{C}_8\text{H}_4\text{O}_4)_6(\text{H}_2\text{O})_4$.

3.2. Catalytic Tests

The hydrogenation reaction of cyclohexene was chosen as a model reaction for rapid determination of the activity of catalysts. To assess the stability of the obtained catalysts, hydrogenation was carried out cyclically. For clarity, the dependences of the rate of hydrogenation of cyclohexene, reduced to g-atm of Pd, on time, for different types of the obtained catalytic systems, are shown in comparison with the industrial analogue of Pd/C (Figure 7). It has been shown that catalytic hydrogenation systems supported by mesoporous MOFs of the $\text{Pd/Zr}_6\text{O}_4(\text{OH})_6(\text{C}_8\text{H}_4\text{O}_4)_6(\text{H}_2\text{O})_4$ and $\text{Pd/Zr}_6\text{O}_4(\text{OH})_4(\text{C}_{12}\text{H}_6\text{O}_4)_6(\text{H}_2\text{O})_{18}$ types demonstrate initial cyclohexene hydrogenation rates higher than the industrial analogue of Pd/C. The activity of $\text{Pd/Zr}_6\text{O}_4(\text{OH})_4(\text{C}_8\text{H}_4\text{O}_4\text{-NH}_2)_6(\text{H}_2\text{O})_{12}$ is comparable with those of the industrial analogue of Pd/C. The next step in the analysis of the catalytic properties of the

obtained systems was the study of the hydrogenation of phenylacetylene and allyl alcohol. It should be noted that the selective hydrogenation of phenylacetylene contained in the styrene monomer raw material is a necessary process for obtaining high quality polystyrene.

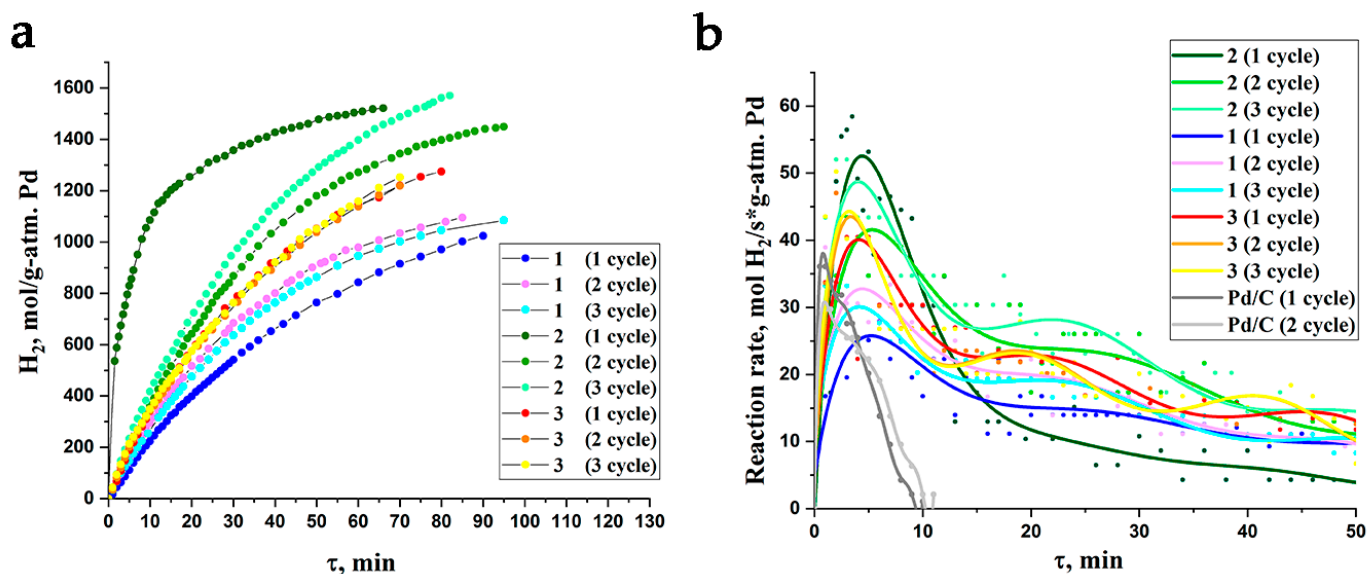


Figure 7. (a) Dependences of hydrogen consumption on time in repeated cycles during the hydrogenation of cyclohexene; (b) the rate of H₂ consumption in repeated cycles (catalyst weight 0.10 g, temperature 40 °C, H₂ pressure 0.1 MPa, medium is isopropanol, initial amount of cyclohexene 7 mmol); 1—Pd/Zr₆O₄(OH)₄(C₈H₄O₄-NH₂)₆(H₂O)₁₂; 2—Pd/Zr₆O₄(OH)₆(C₈H₄O₄)₆(H₂O)₄; 3—Pd/Zr₆O₄(OH)₄(C₁₂H₆O₄)₆(H₂O)₁₈.

During the hydrogenation of phenylacetylene (Figure 8a), the lowest hydrogenation rates are observed for Pd/Zr₆O₄(OH)₄(C₈H₄O₄-NH₂)₆(H₂O)₁₂, which is apparently due to the localization of Pd NPs mainly in MOF pores, i.e., the lowest availability of Pd active sites. Interestingly, when the reaction is carried out in repeated cycles, Pd/Zr₆O₄(OH)₄(C₈H₄O₄-NH₂)₆(H₂O)₁₂ works stably without a decrease in the hydrogenation rate, while the hydrogenation rates of Pd/Zr₆O₄(OH)₆(C₈H₄O₄)₆(H₂O)₄ and Pd/Zr₆O₄(OH)₄(C₁₂H₆O₄)₆(H₂O)₁₈ decrease with each subsequent cycle, so that in the fifth cycle of phenylacetylene hydrogenation the rate of hydrogenation of these systems decreased by 50 and 40% of cycle 1, respectively.

It should be noted that hydrogenation at low temperatures of organic compounds, such as allyl alcohol or its derivatives, is also interesting from the point of view of evaluating the ability of the catalyst to carry out selective conversion, since several directions of the reaction are possible: (1) reduction to the corresponding alcohols, (2) isomerization to saturated or unsaturated aldehydes, (3) hydrodeoxygenation to hydrocarbons [37]. As a result of the hydrogenation experiments (Figures 8 and 9), it was found that the propanol selectivity of the catalysts under consideration was 72–78% at an allyl alcohol conversion of 100%, and the styrene selectivity was approximately 94% at a phenylacetylene conversion of 75–86%. It has been shown that the hydrogenation rates of allyl alcohol for Pd/Zr₆O₄(OH)₄(C₈H₄O₄-NH₂)₆(H₂O)₁₂ are two times higher than those of other systems; in addition, the rate in subsequent cycles increases somewhat, while the rate of hydrogenation for Pd/Zr₆O₄(OH)₆(C₈H₄O₄)₆(H₂O)₄ and Pd/Zr₆O₄(OH)₄(C₁₂H₆O₄)₆(H₂O)₁₈ decreases with each subsequent cycle, so that in the fifth cycle of allyl alcohol hydrogenation the rate of hydrogenation of these systems decreased by 50 and 35% of cycle 1, respectively.

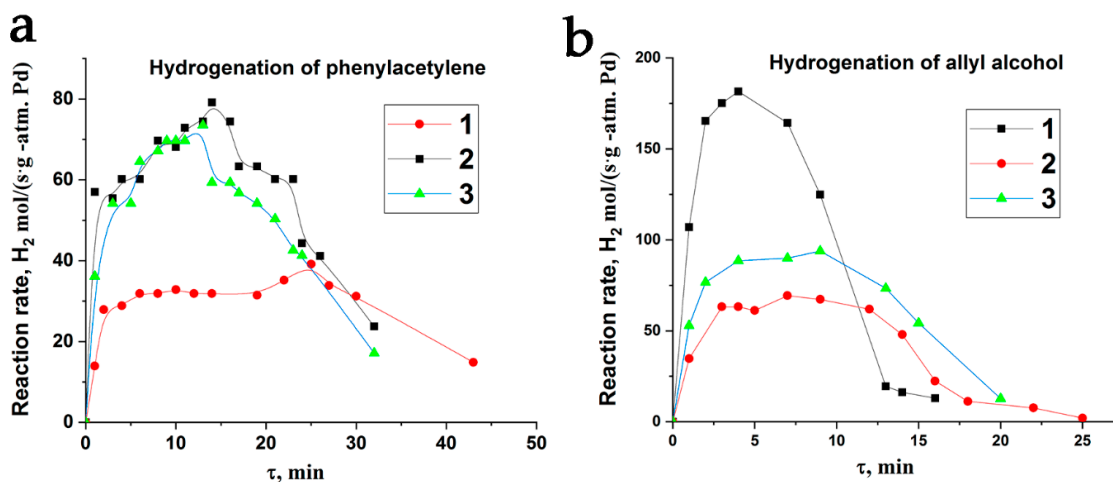


Figure 8. H₂ consumption rate in repeated cycles in the hydrogenation of phenylacetylene (a) and allyl alcohol (b) (Catalyst weight—0.05 g, temperature 40 °C, H₂ pressure—0.1 MPa, ethanol, Vex = 0.25 mL.); 1—Pd/Zr₆O₄(OH)₄(C₈H₄O₄-NH₂)₆(H₂O)₁₂; 2—Pd/Zr₆O₄(OH)₆(C₈H₄O₄)₆(H₂O)₄; 3—Pd/Zr₆O₄(OH)₄(C₁₂H₆O₄)₆(H₂O)₁₈.

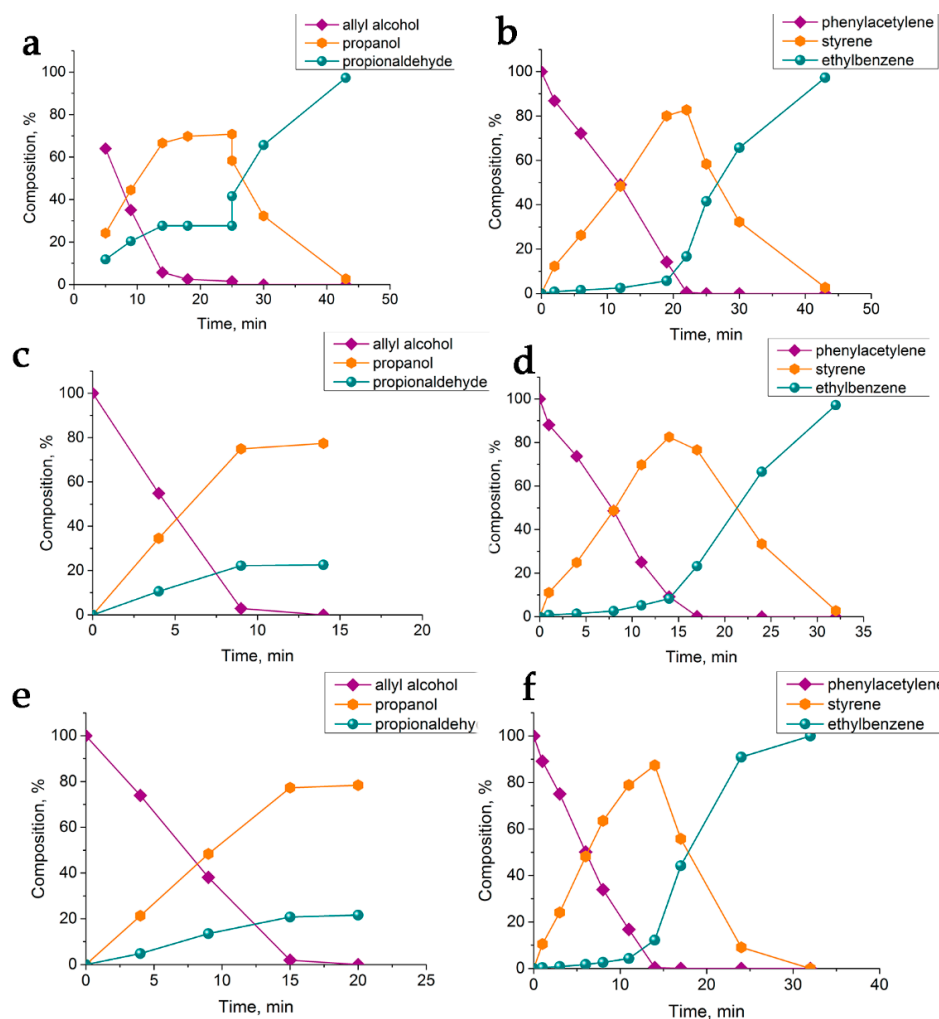


Figure 9. Composition of the hydrogenation reaction mixture at different reaction points: (a,b)—Pd/Zr₆O₄(OH)₄(C₈H₄O₄-NH₂)₆(H₂O)₁₂; (c,d)—Pd/Zr₆O₄(OH)₆(C₈H₄O₄)₆(H₂O)₄; (e,f)—Pd/Zr₆O₄(OH)₄(C₁₂H₆O₄)₆(H₂O)₁₈.

4. Conclusions

As part of the research, a low-temperature rational approach was proposed for the preparation of UiO-type mesoporous MOFs using non-toxic solvents and presynthesized polynuclear zirconium complexes as sources of secondary building blocks. MOFs exhibit permanent porosity, mesoporous structure, and high thermal stability. The MOFs thus obtained have been shown to be suitable for use as a hydrogenation catalyst platform. Thus, palladium-supported catalytic systems based on MOFs constructed from molecules of benzenedicarboxylic acids and their derivatives demonstrate stable catalytic activity in the hydrogenation reaction in repeated cycles, and can operate effectively under mild conditions with comparable hydrogenation rates in comparison with the most well-known industrial analog Pd/C. It was found that the rates of hydrogenation of allyl alcohol in the presence of Pd/Zr₆O₄(OH)₄(C₈H₄O₄-NH₂)₆(H₂O)₁₂ are two times higher than those of other systems; in addition, the rate even slightly increases in subsequent cycles. We hope that the results of this study will contribute to the further development of low-temperature efficient heterogeneous hydrogenation catalysts, which are supported by objects of a completely new type in the field of chemistry and materials science: MOFs, capable of operating efficiently in mild conditions, not inferior to the most well-known industrial analogues of Pd/C.

Author Contributions: Conceptualization, I.E.U. and G.I.D.; methodology, I.E.U., G.I.D. and A.K.Z.; writing—original draft, R.K.B.; writing—review and editing, I.E.U. and G.I.D.; resources, A.K.Z.; investigation, A.V.A., F.U.B., G.V.S. and R.K.B.; visualization, R.K.B.; project administration, G.I.D.; supervision, I.E.U. All authors have read and agreed to the published version of the manuscript.

Funding: The reported study was funded by Russian Foundation for Basic Research (RFBR), project number 20-33-90182.

Data Availability Statement: The data presented in this study are available in the article.

Acknowledgments: This work has been carried out in accordance with the state tasks, state registration AAAAA19119032690060-9, AAAA-A19-119041090087-4 and AAAA-A19-119101590029-0 using the equipment of the Multi-User Analytical Center of IPCP RAS. The authors thank Ivanov A.V., Kurkina E.A. for help in conducting the experiments.

Conflicts of Interest: The authors declare no conflict of interest.

References

1. Mironenko, R.M.; Likhobolov, V.A.; Belskaya, O.B. Nanoglobular Carbon and Palladium–Nanoglobular Carbon Catalysts for Liquid-Phase Hydrogenation of Organic Compounds. *Russ. Chem. Rev.* **2022**, *91*, RCR5017. [\[CrossRef\]](#)
2. Li, Z.; Meng, X. Recent Development on Palladium Enhanced Photocatalytic Activity: A Review. *J. Alloys Compd.* **2020**, *830*, 154669. [\[CrossRef\]](#)
3. Genuino, H.C.; van de Bovenkamp, H.H.; Wilbers, E.; Winkelman, J.G.M.; Goryachev, A.; Hofmann, J.P.; Hensen, E.J.M.; Weckhuysen, B.M.; Bruijninx, P.C.A.; Heeres, H.J. Catalytic Hydrogenation of Renewable Levulinic Acid to γ -Valerolactone: Insights into the Influence of Feed Impurities on Catalyst Performance in Batch and Flow Reactors. *ACS Sustain. Chem. Eng.* **2020**, *8*, 5903–5919. [\[CrossRef\]](#)
4. Argyle, M.; Bartholomew, C. Heterogeneous Catalyst Deactivation and Regeneration: A Review. *Catalysts* **2015**, *5*, 145–269. [\[CrossRef\]](#)
5. Han, Y.; Xu, H.; Su, Y.; Xu, Z.; Wang, K.; Wang, W. Noble Metal (Pt, Au@Pd) Nanoparticles Supported on Metal Organic Framework (MOF-74) Nanoshuttles as High-Selectivity CO₂ Conversion Catalysts. *J. Catal.* **2019**, *370*, 70–78. [\[CrossRef\]](#)
6. Tshuma, P.; Makhubela, B.C.E.; Bingwa, N.; Mehlana, G. Palladium(II) Immobilized on Metal–Organic Frameworks for Catalytic Conversion of Carbon Dioxide to Formate. *Inorg. Chem.* **2020**, *59*, 6717–6728. [\[CrossRef\]](#)
7. Kalmutzki, M.J.; Hanikel, N.; Yaghi, O.M. Secondary Building Units as the Turning Point in the Development of the Reticular Chemistry of MOFs. *Sci. Adv.* **2018**, *4*, eaat9180. [\[CrossRef\]](#)
8. Sopianik, A.A.; Kiskin, M.A.; Kovalenko, K.A.; Samsonenko, D.G.; Dybtsev, D.N.; Audebrand, N.; Sun, Y.; Fedin, V.P. Rational Synthesis and Dimensionality Tuning of MOFs from Preorganized Heterometallic Molecular Complexes. *Dalton Trans.* **2019**, *48*, 3676–3686. [\[CrossRef\]](#)
9. Heu, R.; Ateia, M.; Awfa, D.; Punyapalakul, P.; Yoshimura, C. Photocatalytic Degradation of Organic Micropollutants in Water by Zr-MOF/GO Composites. *J. Compos. Sci.* **2020**, *4*, 54. [\[CrossRef\]](#)
10. Wei, M.; Wan, Y.; Zhang, X. Metal-Organic Framework-Based Stimuli-Responsive Polymers. *J. Compos. Sci.* **2021**, *5*, 101. [\[CrossRef\]](#)

11. Uflyand, I.E.; Naumkina, V.N.; Zhinzhiro, V.A. Nanocomposites of Copper Trimesinate and Graphene Oxide as Sorbents for the Solid-Phase Extraction of Organic Dyes. *J. Compos. Sci.* **2022**, *6*, 215. [[CrossRef](#)]
12. Qin, J.-S.; Yuan, S.; Lollar, C.; Pang, J.; Alsalmeh, A.; Zhou, H.-C. Stable Metal–Organic Frameworks as a Host Platform for Catalysis and Biomimetics. *Chem. Commun.* **2018**, *54*, 4231–4249. [[CrossRef](#)] [[PubMed](#)]
13. Gupta, V.; Mandal, S.K. A Microporous Metal–Organic Framework Catalyst for Solvent-Free Strecker Reaction and CO₂ Fixation at Ambient Conditions. *Inorg. Chem.* **2020**, *59*, 4273–4281. [[CrossRef](#)] [[PubMed](#)]
14. Pascanu, V.; González Miera, G.; Inge, A.K.; Martín-Matute, B. Metal–Organic Frameworks as Catalysts for Organic Synthesis: A Critical Perspective. *J. Am. Chem. Soc.* **2019**, *141*, 7223–7234. [[CrossRef](#)]
15. Jiang, H.-L.; Liu, B.; Akita, T.; Haruta, M.; Sakurai, H.; Xu, Q. Au@ZIF-8: CO Oxidation over Gold Nanoparticles Deposited to Metal–Organic Framework. *J. Am. Chem. Soc.* **2009**, *131*, 11302–11303. [[CrossRef](#)]
16. Yuan, B.; Pan, Y.; Li, Y.; Yin, B.; Jiang, H. A Highly Active Heterogeneous Palladium Catalyst for the Suzuki–Miyaura and Ullmann Coupling Reactions of Aryl Chlorides in Aqueous Media. *Angew. Chem. Int. Ed.* **2010**, *49*, 4054–4058. [[CrossRef](#)]
17. Wang, W.; Chen, S.; Guisasola Cal, E.; Martínez Moro, M.; Moya, S.; Coy, E.; Wang, C.; Hamon, J.-R.; Astruc, D. ZIF-8-Based vs. ZIF-8-Derived Au and Pd Nanoparticles as Efficient Catalysts for the Ullmann Homocoupling Reaction. *Inorg. Chem. Front.* **2020**, *7*, 3945–3952. [[CrossRef](#)]
18. Hicks, K.E.; Rosen, A.S.; Syed, Z.H.; Snurr, R.Q.; Farha, O.K.; Notestein, J.M. Zr₆O₈ Node-Catalyzed Butene Hydrogenation and Isomerization in the Metal–Organic Framework NU-1000. *ACS Catal.* **2020**, *10*, 14959–14970. [[CrossRef](#)]
19. Nagendiran, A.; Pascanu, V.; Bermejo Gómez, A.; González Miera, G.; Tai, C.-W.; Verho, O.; Martín-Matute, B.; Bäckvall, J.-E. Mild and Selective Catalytic Hydrogenation of the C=C Bond in α,β -Unsaturated Carbonyl Compounds Using Supported Palladium Nanoparticles. *Chem. Eur. J.* **2016**, *22*, 7184–7189. [[CrossRef](#)]
20. Bakuru, V.R.; Kalidindi, S.B. Synergistic Hydrogenation over Palladium through the Assembly of MIL-101(Fe) MOF over Palladium Nanocubes. *Chem. Eur. J.* **2017**, *23*, 16456–16459. [[CrossRef](#)]
21. Isaeva, V.I.; Eliseev, O.L.; Chernyshev, V.V.; Bondarenko, T.N.; Vergun, V.V.; Kapustin, G.I.; Lapidus, A.L.; Kustov, L.M. Palladium Nanoparticles Embedded in MOF Matrices: Catalytic Activity and Structural Stability in Iodobenzene Methoxycarbonylation. *Polyhedron* **2019**, *158*, 55–64. [[CrossRef](#)]
22. Wu, H.Q.; Huang, L.; Li, J.Q.; Zheng, A.M.; Tao, Y.; Yang, L.X.; Yin, W.H.; Luo, F. Pd@Zn-MOF-74: Restricting a Guest Molecule by the Open-Metal Site in a Metal–Organic Framework for Selective Semihydrogenation. *Inorg. Chem.* **2018**, *57*, 12444–12447. [[CrossRef](#)] [[PubMed](#)]
23. Fei, H.; Cohen, S.M. Metalation of a Thiocatechol-Functionalized Zr(IV)-Based Metal–Organic Framework for Selective C–H Functionalization. *J. Am. Chem. Soc.* **2015**, *137*, 2191–2194. [[CrossRef](#)] [[PubMed](#)]
24. Kulikov, L.A.; Terenina, M.V.; Kryazheva, I.Y.; Karakhanov, E.A. Unsaturated-Compound Hydrogenation Nanocatalysts Based on Palladium and Platinum Particles Immobilized in Pores of Mesoporous Aromatic Frameworks. *Petr. Chem.* **2017**, *57*, 222–229. [[CrossRef](#)]
25. Zhang, K.; Kim, J.; Kirlikovali, K.O.; Wang, J.; Lee, T.H.; Kim, S.Y.; Varma, R.S.; Jang, H.W.; Farha, O.K.; Shokouhimehr, M. Magnetically Recyclable Nanocomposites via Lanthanide-Based MOFs Grown on Natural Sea Sponge: Screening Hydrogenation of Nitrophenol to Aminophenol. *Mol. Catal.* **2022**, *528*, 112459. [[CrossRef](#)]
26. Aldoshin, S.M.; Dzhardimalieva, G.I.; Pomogailo, A.D.; Abuzin, Y.A. Reactivity of Metal-Containing Monomers 71. Synthesis of Nanosized Quasicrystals and Related Metallopolymer Composites. *Russ. Chem. Bull.* **2011**, *60*, 1871–1879. [[CrossRef](#)]
27. Dzhardimalieva, G.I.; Zharmagambetova, A.K.; Kudaibergenov, S.E.; Uflyand, I.E. Polymer-Immobilized Clusters and Metal Nanoparticles in Catalysis. *Kinet. Catal.* **2020**, *61*, 198–223. [[CrossRef](#)]
28. Sharma, P.; Mukherjee, D.; Sarkar, S.; Mandler, D.; Varma, R.S.; Gawande, M.B.; Zbořil, R.; Sasson, Y. Pd Doped Carbon Nitride (Pd-g-C₃N₄): An Efficient Photocatalyst for Hydrogenation via an Al–H₂O System and an Electrocatalyst towards Overall Water Splitting. *Green Chem.* **2022**, *24*, 5535–5546. [[CrossRef](#)]
29. Rout, D.R.; Senapati, P.; Sutar, H.; Sau, D.C.; Murmu, R. Graphene Oxide (GO) Supported Palladium (Pd) Nanocomposites for Enhanced Hydrogenation. *Graphene* **2019**, *8*, 33–51. [[CrossRef](#)]
30. Howarth, A.J.; Liu, Y.; Li, P.; Li, Z.; Wang, T.C.; Hupp, J.T.; Farha, O.K. Chemical, Thermal and Mechanical Stabilities of Metal–Organic Frameworks. *Nat. Rev. Mater.* **2016**, *1*, 15018. [[CrossRef](#)]
31. Schaate, A.; Roy, P.; Godt, A.; Lippke, J.; Waltz, F.; Wiebcke, M.; Behrens, P. Modulated Synthesis of Zr-Based Metal–Organic Frameworks: From Nano to Single Crystals. *Chem. Eur. J.* **2011**, *17*, 6643–6651. [[CrossRef](#)] [[PubMed](#)]
32. Valenzano, L.; Civalieri, B.; Chavan, S.; Bordiga, S.; Nilsen, M.H.; Jakobsen, S.; Lillerud, K.P.; Lamberti, C. Disclosing the Complex Structure of UiO-66 Metal Organic Framework: A Synergic Combination of Experiment and Theory. *Chem. Mater.* **2011**, *23*, 1700–1718. [[CrossRef](#)]
33. Hennig, C.; Weiss, S.; Kraus, W.; Kretzschmar, J.; Scheinost, A.C. Solution Species and Crystal Structure of Zr(IV) Acetate. *Inorg. Chem.* **2017**, *56*, 2473–2480. [[CrossRef](#)] [[PubMed](#)]
34. Harraz, F.A.; El-Hout, S.E.; Killa, H.M.; Ibrahim, I.A. Palladium Nanoparticles Stabilized by Polyethylene Glycol: Efficient, Recyclable Catalyst for Hydrogenation of Styrene and Nitrobenzene. *J. Catal.* **2012**, *286*, 184–192. [[CrossRef](#)]
35. Yan, F.; Wang, Q.; Wang, F.; Huang, Z. Study on Energy Storage Properties of Metal–Organic Frameworks Nanofluids (UIO-67/Water and UIO-67/Methanol) by an Experimental and Theoretical Method. *J. Mater. Sci.* **2021**, *56*, 10008–10017. [[CrossRef](#)]

36. Pangestu, A.; Lestari, W.W.; Wibowo, F.R.; Larasati, L. Green Electro-Synthesized MIL-101(Fe) and Its Aspirin Detoxification Performance Compared to MOF-808. *J. Inorg. Organomet. Polym.* **2022**, *32*, 1828–1839. [[CrossRef](#)]
37. Di Pietrantonio, K.; Coccia, F.; Tonucci, L.; d'Alessandro, N.; Bressan, M. Hydrogenation of Allyl Alcohols Catalyzed by Aqueous Palladium and Platinum Nanoparticles. *RSC Adv.* **2015**, *5*, 68493–68499. [[CrossRef](#)]